Submitted for the special HST ERO issue of the Astrophysical Journal Letters

UV Absorption Lines from High-Velocity Gas in the Vela Supernova Remnant: New Insights from STIS Echelle Observations of HD72089[1]

Edward B. Jenkins[2], Todd M. Tripp[2], Edward L. Fitzpatrick[2], Don Lindler[3,4], Anthony C. Danks[5,4], Terrence L. Beck[3,4], Charles W. Bowers[4], Charles L. Joseph[6], Mary Elizabeth Kaiser[7,4], Randy A. Kimble[4], Stephen B. Kraemer[8,4], Richard D. Robinson[9,4], J. Gethyn Timothy[10], Jeff A. Valenti[11], Bruce E. Woodgate[4]

ABSTRACT

The star HD72089 is located behind the Vela supernova remnant and shows a complex array of high and low velocity interstellar absorption features arising from shocked clouds. A spectrum of this star was recorded over the wavelength range 1196.4 Å to 1397.2 Å at a resolving power $\lambda/\Delta\lambda = 110,000$ and signal-to-noise ratio of 32 by STIS on the Hubble Space Telescope. We have identified 7 narrow components of C I and have measured their relative populations in excited fine-structure levels. Broader features at heliocentric velocities ranging from -70 to $+130$ km s^{-1} are seen in C II, N I, O I, Si II, S II and Ni II. In the high-velocity components, the unusually low abundances of N I and O I, relative to S II and Si II, suggest that these elements may be preferentially ionized to higher stages by radiation from hot gas immediately behind the shock fronts.

---

[1]Based on observations with the NASA/ESA *Hubble Space Telescope* obtained at the Space Telescope Science Institute, which is operated by AURA, Inc. under NASA contract NAS5−26555. The analysis was supported by NASA Grant NAG5-30110 to Princeton University.

[2]Princeton University Observatory, Princeton, NJ 08544

[3]Adv. Comp. Concepts

[4]Code 681, NASA Goddard Space Flight Center, Greenbelt, MD 20771

[5]Hughes/STX

[6]Physics & Astronomy, P.O. Box 849, Rutgers University, Piscataway, NJ 08855

[7]Dept. of Physics and Astronomy, Johns Hopkins University

[8]Dept. of Physics, Catholic University

[9]CSC

[10]CRESS, York University, North York, Ontario M3J 1P3, Canada

[11]JILA, Campus Box 440, University of Colorado, Boulder, CO 80309−0440

Subject headings: ISM: abundances — ISM: individual (Vela supernova remnant) — ISM: kinematics and dynamics — shock waves — stars: individual (HD 72089) — supernova remnants

1. Introduction

The large number of bright, early-type stars within or behind the Vela supernova remnant (SNR) makes this remnant especially well suited for the study of high velocity absorption features from shocked gases. An especially interesting example is the star HD72089, discovered by Jenkins & Wallerstein (1984) to have at least six distinct velocity components in Ca II. HST observations of HD72089 using the G160M grating on GHRS ($\lambda/\Delta\lambda = 20,000$) revealed the presence of high velocity C I features with extraordinarily strong absorption coming from excited fine-structure levels, indicating the gas is strongly compressed (Jenkins & Wallerstein 1995, hereafter JW95). In their study of gas-phase element abundances in the halo of the Galaxy, Jenkins & Wallerstein (1996, hereafter JW96) used the pattern of element abundances in the high velocity components toward HD72089 as a comparison standard for reduced depletions caused by the destruction of grains in shocks. With new observations of this star covering the spectral region from 1196.4 Å to 1397.2 Å by STIS on HST, we are able to arrive at more accurate results for the nature of the high velocity gas.

2. Data

HD72089 is a star with $V = 8$ and a spectral classification B5 II-III (Houck 1978) that is about 1.7 kpc away from us, located behind the western edge of the Vela SNR. We present in this Letter observations of this star taken on 30 May 1997 0022−0354 UT[12] to demonstrate the performance of the high-resolution UV echelle spectrograph (E140H mode) on STIS with the 0.2×0.09 arc-sec entrance aperture.

Photoevents registered by the MAMA detector were recorded in the time-tag mode. We created a 2048x2048 Hi-Res image (2 samples per MAMA pixel) with corrections for the position of each time-tagged count to compensate for (1) the orbital Doppler motion (amplitude = 10 Hi-Res pixels) and (2) the motion caused by thermal distortions (0.2 Hi-Res pixels per hour, measured from the slow drift of the spectral lines within the data). Our spectra were taken from simple, unweighted extractions with background levels defined by the bottoms of obviously

[12]Archive exposure index numbers O40O01P9M, PDM and PHM, with integration times of 1420, 2560 and 2560 s, respectively.

saturated lines. In cases where lines of interest appeared twice in adjacent orders, the overlapping coverages were co-added.

The wavelength scale was computed using a pre-launch dispersion relation corrected for a zero point wavelength shift computed from a wavelength calibration observation taken with the data. The precision of this scale is shown by the excellent agreement for the derived wavelengths of narrow features seen in two different orders. Also, the velocities of our C I components agree to within 2 km s^{-1} (rms error) with those of Na I observed by Danks & Sembach (1995).

Except in the vicinity of the strong stellar Ly-α line, our derived spectrum has a signal-to-noise ratio of about 32. From a narrow line of Cl I (not discussed here), we estimate that the instrumental profile is a Gaussian with a FWHM equal to $\lambda/1.1 \times 10^5$. In this Letter, we focus principally on the absorption lines of C I (§3) with their noteworthy levels of fine-structure excitation, and in §4 we report on some key elements that show up in ionization stages that are favored in normal H I regions.

3. High-Excitation C I

In the ISM, the excited $^3P_1$ and $^3P_2$ fine-structure levels (denoted C I* and C I**) in the ground state of C I can be populated by collisions with neutral hydrogen atoms, electrons and protons (Bahcall & Wolf 1968; Jenkins & Shaya 1979; Keenan 1989; Roueff & Le Bourlot 1990). In the previous *HST* study of HD 72089, JW95 measured remarkably strong C I* and C I** lines in the component at $v = +121$ km s^{-1}. The large implied gas pressure suggested that this C I absorption arises in compressed gas following a shock inside a cloud that had been hit by the supernova blast wave. Our new STIS observations of HD 72089 have substantially improved resolution and provide an opportunity to verify and refine the results of JW95.

We analyzed C I multiplets near 1277 Å, 1280 Å, and 1329 Å using a component fitting technique (Spitzer & Fitzpatrick 1993; Fitzpatrick & Spitzer 1997) that minimizes the χ^2 between the fit and the data to determine the set of velocity centroids, b-values, and column densities, assuming the original intensities were convolved with an instrumental line spread function consisting of a Gaussian with FWHM = 4 Hi-Res pixels. A comparison of the derived fits with the recorded spectra near the 1277 Å and 1329 Å C I absorption complexes is shown in Figure 1. The parameters for the 7 individual absorption components are given in Table 1. The associated 1σ errors include the effects of random photon noise, residual fixed pattern noise and uncertainties in determining the continuum. Since we relied on empirically derived backgrounds, there may be additional systematic errors at the ∼5% level. Such errors, however, will tend to shift all of the C I, C I*, and C I** column densities in a given multiplet in the same direction and thus will not significantly affect the derived population ratios, f_1 and f_2, listed in the last two columns of the table. Figure 1 indicates that many lines are free from blending, and consequently the component parameters are well-constrained by the data.

Table 1. Profile Fitting Results: Component Velocities, Doppler Parameters, and Column Densities for C I, C I*, and C I**

Component Number	$v_\odot$[a] (km s^{-1})	b[b] (km s^{-1})	log N(C I)	log N(C I*)	log N(C I**)	f_1[c]	f_2[c]
1.....	3.2±0.1	1.6±0.3	12.84±0.02	12.29±0.08	< 11.7[d]	0.22	< 0.054
2.....	6.5±0.2	6.3±0.7	12.96±0.02	13.06±0.02	12.92±0.02	0.39	0.29
3.....	16.7±0.1	2.2±0.4	12.78±0.02	11.54±0.41	< 11.6[d]	0.05	< 0.059
4.....	26.2±0.1	5.3±0.6	13.11±0.02	12.85±0.03	12.60±0.04	0.29	0.17
5.....	35.4±0.1	3.2±0.2	12.94±0.02	12.97±0.01	12.59±0.03	0.43	0.18
6.....	90.5±0.2	5.0±0.7	12.38±0.06	12.50±0.04	12.72±0.02	0.29	0.49
7.....	120.9±0.1	2.9±0.2	12.36±0.03	12.79±0.02	13.00±0.01	0.34	0.54

[a]Errors in the formal fits exclude systematic uncertainties in the STIS wavelength scale and laboratory wavelengths. Subtract 16.9 km s^{-1} to obtain LSR velocities.

[b]Errors do not include the uncertainty in the assumed width of the instrumental line spread function.

[c]The relative populations of the C I fine-structure levels in the notation of Jenkins & Shaya (1979): $f_1 = N(\mathrm{C\ I^*})/N(\mathrm{C\ I})_{\mathrm{total}}$ and $f_2 = N(\mathrm{C\ I^{**}})/N(\mathrm{C\ I})_{\mathrm{total}}$.

[d]Formal result for the column density is a small negative number; upper limit quoted here reflects that result plus a 2σ error.

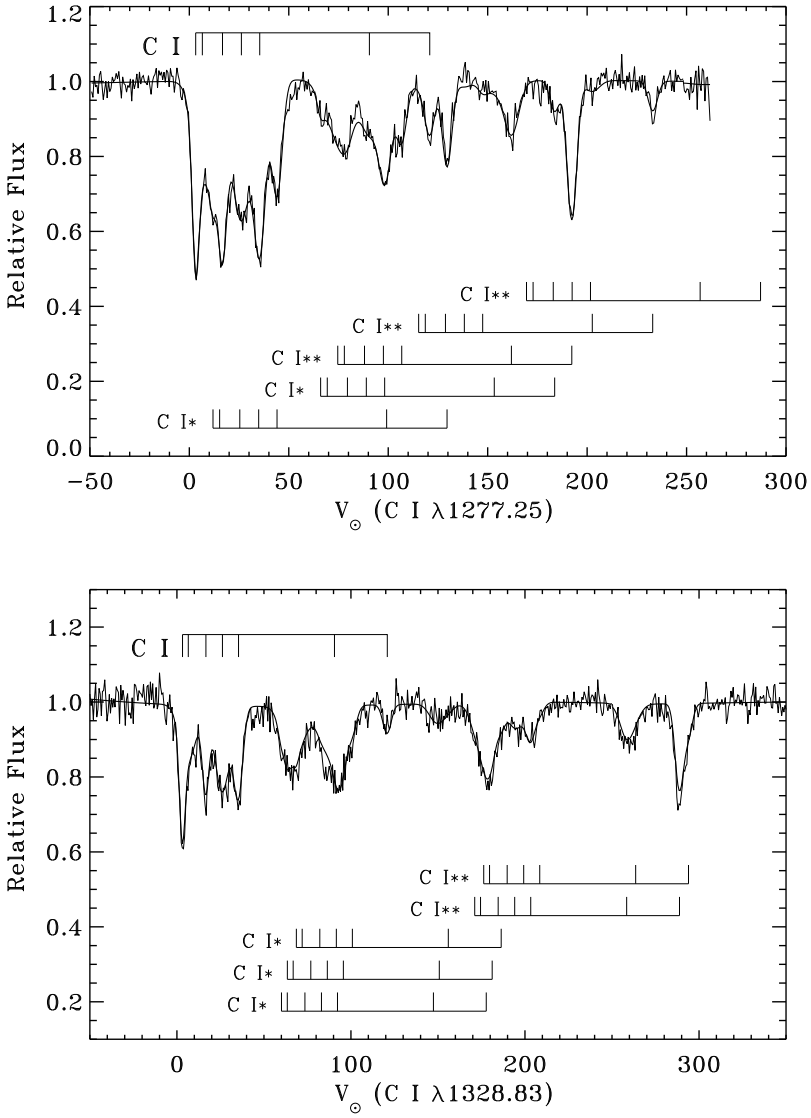

Fig. 1.— Absorption profiles in the heliocentric velocity frame of the (top) C I 1277 Å and (bottom) C I 1329 Å multiplets. The profile fits based on the component parameters in Table 1 are overplotted on the data, and the velocities of the seven components in the various C I, C I*, and C I** lines in these multiplets are indicated. The C I multiplet near 1280 Å was also fitted but is not shown here.

At sufficiently high densities in a warm gas, the level populations approach their relative statistical weights, i.e., 1:3:5, so that $f_1 \rightarrow 0.33$ and $f_2 \rightarrow 0.56$. We confirm the determination by JW95 that this condition is found for the component at the highest velocity (our Component 7). We find that some components at low and intermediate velocities (Components 2, 4 and 6) have values of f_1 and f_2 that must arise from blends of unresolved components, each with differing degrees of C I excitation caused by very different pressures or levels of ionization.[13] This conclusion is supported by the slightly larger b-values of these components. Finally, Component 3 has an unusually low excitation. Gas within this region would have a pressure $p/k \approx 1300$ cm^{-3}K if $T = 300$K (and electron and proton densities are low enough to be neglected), but p/k could be as large as 7400 cm^{-3}K at the upper limit for temperature $T = mb^2/2k = 3400$K indicated by our measurement of the line width.

4. Selected Atoms and Ions

The general character of the velocity components for ionization stages of elements that have an IP > 13.6 eV is very different from the narrow components seen in C I. C I emphasizes mostly regions that have large internal densities, while lines from such species as C II, N I, O I, Si II, S II, and Ni II are likely to arise from a much broader range of conditions in generally lower density clouds. It is no surprise that the latter group display lines that have a broad velocity extent with virtually no evidence for narrow, unresolved substructures (see below). For this reason, we choose to analyze the features in the context of their apparent optical depths τ_a as a function of radial velocity v (Savage & Sembach 1991; Jenkins 1996), a concept that is more general than component fitting. For the line complexes of N I, O I, Si II and S II, the saturation at low velocities was too large to allow any column density determinations (see Fig. 2). The lines of C II and C II* near 1335 Å were hopelessly saturated at all velocities.

To within the noise fluctuations, the high-velocity components of the weakest lines of N I, S II and Si II* yield values of apparent column density, $N_a(v) = 3.768 \times 10^{14} \tau_a(v)/(f\lambda)$ cm^{-2}(km s^{-1})$^{-1}$, that are consistent with those from the strongest lines. The lines for these three species cover ranges of $f\lambda$ that differ by factors of 3, 3 and 10, respectively. Unfortunately, the strong line of Si II at 1260.422 Å has very serious interference from the line of Fe II at 1260.533 Å, so we can not compare it with the weaker feature at 1304.370 Å. The good agreements indicate that the derived $\tau_a(v)$'s are not underestimated because of the presence of saturated substructures that are not resolved by the instrument (and this probably applies to many species other than N I, S II and Si II*). Thus it is not necessary to invoke the special correction procedure outlined by Jenkins (1996), and henceforth we will replace $N_a(v)$ with $N(v)$, the *true* column density per unit velocity.

[13] See §IVa of Jenkins & Shaya (1979) for a simple geometrical method of interpreting possible combinations of absorbing regions that blend together and produce measured (f_1, f_2) that are inconsistent with a single source region.

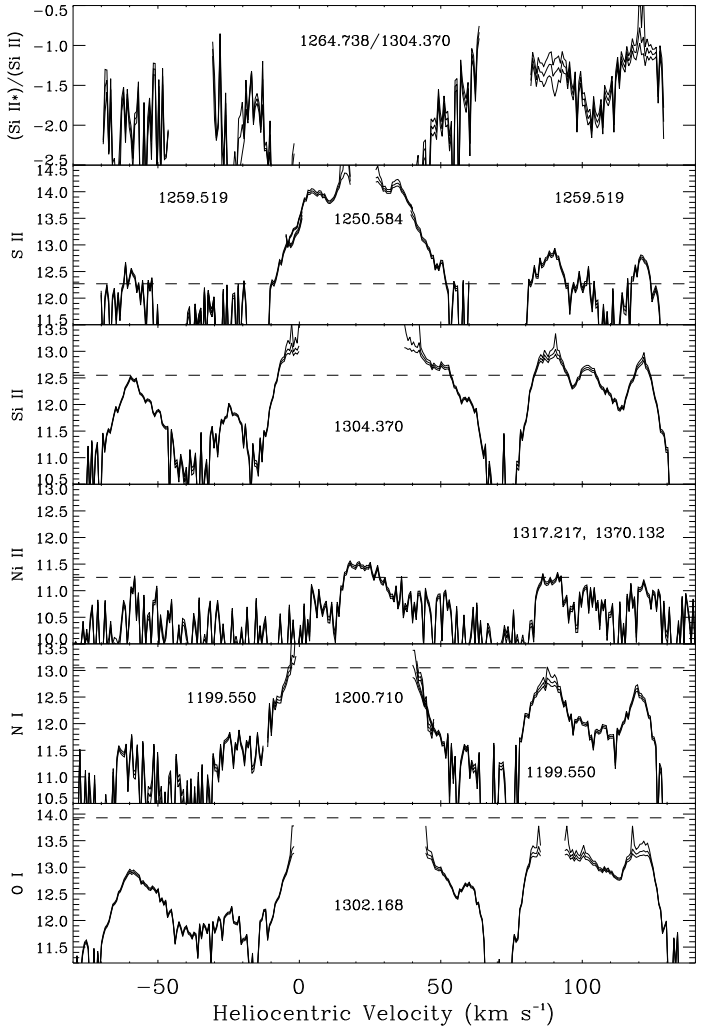

Fig. 2.— Plots of $\log N(v)$ for 5 species, as labeled (lower panels), and the relationship $\log[N(\mathrm{Si\ II^*})/N(\mathrm{Si\ II})]$ (top panel) – an indicator of the local electron density, n_e (see Eq. 1). The dashed lines (drawn at an arbitrary level for S II) represent levels that are consistent with the elements' cosmic abundance relative to S, i.e., the fact that the peaks of some species (e.g. N I and O I) are substantially displaced downwards from the dashed lines relative to their counterparts for S II indicates that these elements are less abundant than expected, relative to S. Transition f-values were taken from Morton (1991), except for Si II (Spitzer & Fitzpatrick 1993) and Si II* (Luo, Pradhan, & Shull 1988).

The lowest 5 panels in Fig. 2 show $\log N(v)$ for S II, Si II, Ni II, N I and O I, with the ordering of these species being based on an *apparent* decrease in general abundances below their respective cosmic abundances (Anders & Grevesse 1989; Grevesse & Noels 1993) (but see §5), assuming that sulfur is undepleted (Fitzpatrick & Spitzer 1997). The magnitudes of these deficiencies for the most negative and the most positive velocity peaks are listed in the second column of Table 2. For some species, there are velocity regions where the features are either lost in the noise or badly saturated. We have omitted these parts of the tracings from the figure. Absorption by low-velocity P II λ1301.874 could be adding to the right-hand side of the O I peak centered at -60 km s^{-1}. The plotted lines consist of a superposition of three determinations (often overlapping) — a middle line that represents our best estimate for $\log N(v)$ that is flanked by ones that represent the extremes that could be caused by worst combinations of systematic errors (1σ) in either the zero intensity level or the placement of the continuum level (errors caused by noise are *not included*, as one can estimate these from the size of the random wiggles in the tracings).

5. Ionization by Radiation from Shocks

The strong deficiencies of N and O shown in Table 2 are inconsistent with previous findings for the general ISM that indicate these two elements are only mildly depleted (Hibbert, Dufton, & Keenan 1985; Cardelli, Savage, & Ebbets 1991; Cardelli et al. 1991; Meyer et al. 1994). One possible interpretation of this phenomenon is that ionizing radiation from nearby shock fronts moves the atoms to higher, unseen stages of ionization. To investigate the plausibility of this idea for these two species plus others, we performed a simple exercise. For representative values of $N(\text{Si II}^*)/N(\text{Si II})$ of 10^{-2} and $10^{-1.15}$ for the components centered at -58 and $+121$ km s^{-1}, respectively, we used the collision cross section and radiative decay rate of the upper fine-structure level given by Keenan et al. (1985) to obtain the electron density as a function of temperature,

$$n_e = \frac{8.97T^{0.5}[N(\text{Si II}^*)/N(\text{Si II})]}{\exp(-413\text{K}/T) - 0.5[N(\text{Si II}^*)/N(\text{Si II})]} \ . \tag{1}$$

We then used the $13 - 54$ eV ionizing radiation field of Shull & McKee (1979) for a shock with a velocity $v_s = 100$ km s^{-1} and preshock density $n_0 = 10$ cm^{-3} (see JW95) and evaluated the ionization equilibrium between the visible stages in Table 2 (denoted with a subscript 1) and the next two higher ionization states (subscripts 2 and 3) to obtain the ratio,

$$R \equiv \frac{n_1}{n_1 + n_2 + n_3} = \left\{ 1 + \frac{(\Gamma_1 + \delta_2 n_e)[\Gamma_2 + (\alpha_2 n_e + \delta_3' n_{\rm H})]}{(\alpha_1 n_e + \delta_2' n_{\rm H})(\alpha_2 n_e + \delta_3' n_{\rm H})} \right\}^{-1} , \tag{2}$$

with $n_{\rm H} = n_e^2 \alpha_{n\geq 2,{\rm H}}/\Gamma_{\rm H}$. Γ_1 and Γ_2 are the photo-ionization rates out of the two lower stages, using cross sections calculated from the analytic approximations of Verner, et al. (1996) [and Verner & Yakovlev (1995) for Ni]. The recombination coefficients α_1 and α_2 were evaluated from the parameters for the fitting equations given by Shull & Van Steenberg (1982) [and Aldrovandi

Table 2. Observed and Calculated Deficiencies

		$\log R$ (from Eq. 2)	
Species[a]	$\log(A/\mathrm{S\ II})_{\mathrm{obs}} - \log(A/\mathrm{S})_{\odot}$	$\log T = 2.7$	$\log T = 3.4$
N I (−58)	−1.72	−2.04[b]	−2.39
N I (+121)	−0.87	−0.93[b]	−1.17
O I (−58)	−1.14[c]	−1.35	−2.01
O I (+121)	−0.90	−0.42	−0.87
Al II (−58)	−0.58[d]	−0.07[b]	−0.18
Al II (+121)	−0.66[d]	e	−0.03
Si II (−58)	−0.36	e	−0.03
Si II (+121)	−0.21	e	0.00
S II (−58)	(0.00)	−0.12[b]	−0.24
S II (+121)	(0.00)	e	−0.04
Fe II (−58)	−0.82[d]	f	−0.75
Fe II (+121)	−0.35[d]	e	−0.02
Ni II (−58)	g	f	−0.74
Ni II (+121)	−0.51	e	−0.03

[a]Numbers in parentheses identify velocity components: "−58" applies to $\int N(v)dv$ (for column 2) over the heliocentric velocity range −70 to −45 km s^{-1} where Eq. 1 gives $n_e = 4.6$ and 5.3 cm^{-3} for $\log T = 2.7$ and 3.4, respectively, and "+121" applies to the range +112 to +130 km s^{-1} ($n_e = 35$ and 39 cm^{-3}).

[b]Numbers neglect charge exchange reactions with H because the fitting formulae for cross sections are not valid for $T < 10^3$K, but judging from the small effect at $10^{3.4}$K, the omission of these reactions is probably not important.

[c]May include some contamination from the 1301.874Å feature of P II at low velocities.

[d]Column density from JW96, compared to S II measured in this investigation.

[e]Since $\log R > -0.1$ at $T = 10^{3.4}$K, the same probably applies here, even though we can not include charge exchange reactions.

[f]Charge exchange reactions have a big effect at $T = 10^{3.4}$K, thus we have no confidence in quoting a number that neglects charge exchange at lower T.

[g]Some Ni II is present, but the absorption feature is too weak to measure.

& Péquignot (1974) for Al]. Values for the charge exchange rates δ_3' ($X_3 + H \rightarrow X_2 + H^+$) and δ_2' ($X_2 + H \rightarrow X_1 + H^+$) were derived from the fits given by Kingdon & Ferland (1996). Unfortunately, for all elements except oxygen, these charge exchange fits are valid only for $T > 10^3$K. We neglected any possible self-absorption of the ionizing radiation by neutral hydrogen, and we did not include charge exchange with He. At $\log T \approx 2$ only the lower of the two Si II*/Si II cases has an acceptable solution in Eq. 1 (giving $n_e = 80$ cm^{-3}) and values of $\log R$ were about equal to 0 for all species except for N I, where $\log R = -0.32$. Values of $\log R$ at two representative higher temperatures are given in columns 3 and 4 of Table 2. At temperatures much above those given in the table, collisional ionization becomes important. Post-shock gases that are cooling radiatively through temperatures of order 10^4K can likewise exhibit depressions of O I and N I (Trapero et al. 1996; Benjamin & Shapiro 1997).

The results shown in Table 2 indicate that the apparent deficiencies of O and N in the high-velocity components might be due to ionization by radiation from the associated immediate post-shock gas and/or nearby shocks. They also indicate that measurements of Fe II and Ni II in such components could, to a lesser extent, be under-representing the true gas-phase abundances of these elements when the electron densities are low. Measurements of Al II, Si II and S II would still yield reliable abundances, and thus our observed 0.6 dex deficiency of Al II indicates that this element may still be locked up in the remnants of the dust grains that survive the passage of a shock (note that JW96 saw very low amounts of Al III at high velocity).

REFERENCES

Aldrovandi, S. M. V., & Péquignot, D. 1974, Rev. Brasil. de Fisica, 4, 491

Anders, E., & Grevesse, N. 1989, Geochim. Cos. Acta, 53, 197

Bahcall, J. N., & Wolf, R. A. 1968, ApJ, 152, 701

Benjamin, R. A., & Shapiro, P. R. 1997, ApJS, submitted

Cardelli, J. A., Savage, B. D., & Ebbets, D. C. 1991, ApJ, 383, L23

Cardelli, J. A., Savage, B. D., Bruhweiler, F. C., Smith, A. M., Ebbets, D. C., Sembach, K. R., & Sofia, U. J. 1991, ApJ, 377, L57

Danks, A. C., & Sembach, K. R. 1995, AJ, 109, 2627

Fitzpatrick, E. L., & Spitzer, L. 1997, ApJ, 475, 623

Grevesse, N., & Noels, A. 1993, in Origin and Evolution of the Elements, ed. N. Prantzos, E. Vangioni-Flam, & M. Cassé (Cambridge: Cambridge Univ. Press), p. 15

Hibbert, A., Dufton, P. L., & Keenan, F. P. 1985, MNRAS, 213, 721

Houck, N. 1978, Michigan Catalogue of Two-Dimensional Spectral Types for the HD Stars, (Ann Arbor: Univ. of Michigan)

Jenkins, E. B. 1996, ApJ, 471, 292

Jenkins, E. B., & Shaya, E. J. 1979, ApJ, 231, 55

Jenkins, E. B., & Wallerstein, G. 1995, ApJ, 440, 227 (JW95)

— 1996, ApJ, 462, 758 (JW96)

Jenkins, E. B., Wallerstein, G., & Silk, J. 1984, ApJ, 278, 649

Keenan, F. P. 1989, ApJ, 339, 591

Keenan, F. P., Johnson, C. T., Kingston, A. E., & Dufton, P. L. 1985, MNRAS, 214, 37p

Kingdon, J. B., & Ferland, G. J. 1996, ApJS, 106, 205

Luo, D., Pradhan, A. K., & Shull, J. M. 1988, ApJ, 335, 498

Meyer, D. M., Jura, M., Hawkins, I., & Cardelli, J. A. 1994, ApJ, 437, L59

Morton, D. C. 1991, ApJS, 77, 119

Roueff, E., & Le Bourlot, J. 1990, A&A, 236, 515

Savage, B. D., & Sembach, K. R. 1991, ApJ, 379, 245

Shull, J. M., & McKee, C. F. 1979, ApJ, 227, 131

Shull, J. M., & Van Steenberg, M. 1982, ApJS, 48, 95

Spitzer, L., & Fitzpatrick, E. L. 1993, ApJ, 409, 299

Trapero, J., Welty, D. E., Hobbs, L. M., Lauroesch, J. T., Morton, D. C., Spitzer, L., & York, D. G. 1996, ApJ, 468, 290

Verner, D. A., & Yakovlev, D. G. 1995, A&AS, 109, 125

Verner, D. A., Ferland, G. J., Korista, K. T., & Yakovlev, D. G. 1996, ApJ, 465, 487